SUPPLEMENTARY INFORMATION

February 19, 2020

Contents

A Prony Series

A.1 Introduction

The discrete data of E' vs. log f were first obtained from a DMA experiment. The approach to produce a Prony Series data is to fit these data into the Generalized Maxwell Model, which enables an optimal curve to be constructed and fit to the experimental data.

A.2 Calculation Theorem

There is a relation between the variations of E' and and the retardation time spectrum as a function of frequency. Relaxation and retardation time spectra can be calculated exactly from the plot of stress relaxation by using simple Alfrey Approximations in which the exponential term for a single Maxwell unit is replaced by a step function [1]. The exponential term is generally expressed as

$$E(t) = [E_r] + \int_{-\infty}^{+\infty} H(\tau) \exp\left(\frac{-t}{\tau}\right) d(\ln\tau)$$

$$\text{where } H(\tau) = \left[\frac{d\, E(\omega)}{d \log\omega}\right]_{t=\tau} \tag{A1}$$

If we assume that $e^{-t/\tau} = 0$ up to the time $\tau = t$, and $e^{-t/\tau} = 1$ for $\tau > t$. We can write

$$E(t) = [E_r] + \int_{-\ln\tau}^{+\infty} H(\tau)\, d(\ln\tau) \tag{A2}$$

The relaxation time spectrum is expressed as an approximation in terms of the real and imaginary parts of the complex modulus

$$H(\tau) = \left[\frac{d\,E'(\omega)}{d\log\omega}\right]_{\frac{1}{\omega}=\tau} = \frac{2}{\pi}\left[E''(\omega)\right]_{\frac{1}{\omega}=\tau} \tag{A3}$$

The relationship between storage modulus and relaxation time spectrum are illustrated diagrammatically for the case of a single relaxation transition in Figure A.1. The distribution of time spectrum for the model is the derivative of a continuous distribution of storage modulus. The element of area at log ω: $H(\tau) \cdot \mathrm{d}\,(\log\omega)$ represents the local strength of the relaxation at log ω axis. The integrated area represents a single Maxwell element, and equals the strength contribution to entire set of Maxwell elements.

The Prony Series is governed by the integration of all individual integral areas from the time spectrum patterns. The individual time spectrum ω and τ can be replaced by symbol of time t and frequency f. The distribution of relaxation time $H(t)$ is derivative by fitting the discrete data in the plot of storage modulus against logarithm of frequency, further the shape of the $H(t)$ function are divided into 60 pieces presenting 60 Maxwell elements individually. The left endpoint (i.e. low frequency) in primary plot is closed as the value of first elastic element to form an eventual Generalized Maxwell Model.

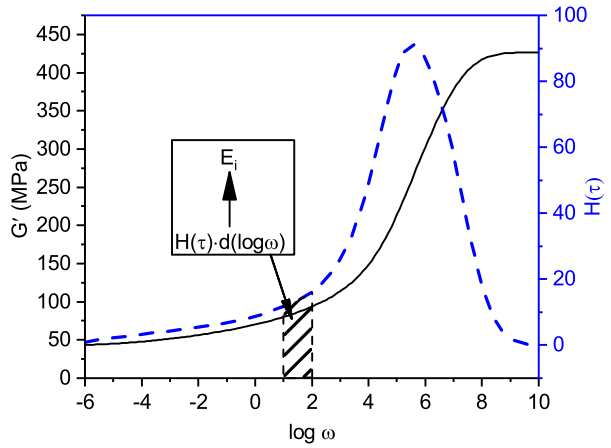

Figure A.1: Alfrey Approximations

A.3 Prony Series at Different Temperatures

The Prony series can be produced from different reference temperature, such as 25, 22.5, 18.7 and 16.8 °C, to match the real experimental temperatures. The optimal curve fitting was restructured by substituting all 61 sets of parameters into Generalized Maxwell Model followed Eq. A4 and Eq. A5. The experimental data and Prony fits are shown in Figure 5 and Figure 6. in the body text.

$$E'(\omega) = E_0 + \sum_{i=1}^{M} E_i \frac{\tau_i{}^2\omega^2}{1+\tau_i{}^2\omega^2} \tag{A4}$$

$$E''(\omega) = \sum_{i=1}^{M} E_i \frac{\tau_i\omega}{1+\tau_i{}^2\omega^2} \tag{A5}$$

B Modelling of Bending and Compression Experiments

B.1 Introduction of Timoshenko Beam Theory

The goal of using beam theory is to simplify the mechanical analysis of beams in the DMA experiment. The common-used beam theory is Euler-Bernoulli beam theory, which can be applied for small deflections if the beam length is much larger than its depth. However, the problem with Euler-Bernoulli beam theory is that it is inaccurate for deep beams, for which shear deformation must be included. Timoshenko beam theory is then applied to include the effect of shear deformation which is ignored in Euler-Bernoulli beam theory. We are here interested the effect of load acting transverse to the longitudinal axis of the beam. The basic assumptions for Timoshenko beam theory are

- The longitudinal axis of the unloaded beam is straight.
- All applied loads act transverse to the longitudinal axis.
- All deformations and strains are small. Hooke's law can be used to relate stresses and strains.
- Plane cross sections, which are initially normal to the longitudinal axis, will remain plane after deformation.

To analyse the DMA test, energy principles, the stiffness matrix, and Green's functions [2] are formulated to solve a typical Timoshenko beam problem in which the beam has a downward unit point load acting at location $x = a$, $\delta = \mu$ (shown in Figure B.1). The point load is represented as a

delta function: $\omega(x) = -\delta(x-a)$. In terms of the dimensionless variable ξ (0<ζ<1), we set $\mu = a/L$. The delta function obeys the scaling property

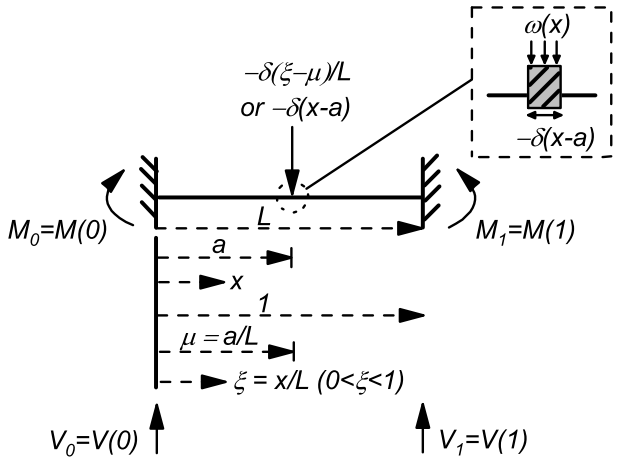

Figure B.1: The simplified bending mechanism of Timoshenko beam in DMA

$$\delta(x-a) = \delta\left[\frac{1}{L}(\xi-\mu)\right] = \frac{1}{L}\delta(\xi-\mu) \tag{B1}$$

Thus we write: $\mu(\xi) = -\delta(\xi-\mu)/L$. We also require the fact that the integral of the delta function is the Heavside function

$$\int_0^{\zeta} \delta(\tau-\mu)\, d\mu = H(\zeta-\mu) = \begin{cases} 1 & \text{if } \zeta \geq \mu \\ 0 & \text{if } \zeta < \mu \end{cases} \tag{B2}$$

Successive integrals of the Heaviside function are given by the formula

$$\int_0^{\zeta} (\tau-\mu)^n H(\tau-\mu)\, \mathrm{d}\tau = \frac{(\zeta-\mu)^{n+1}}{n+1} H(\tau-\mu)$$

$$\text{where } n \geq 0 \tag{B3}$$

These properties allow explicit integration of the solutions below to apply Green's function. The shear force is computed to be

$$V(\zeta) = L \int_0^{\zeta} \omega(\tau)\, d\tau + V_0 \tag{B4}$$

$$V(\zeta) = L \int_0^{\zeta} -\frac{1}{L}\delta(\tau - \mu)\, d\tau + V_0 \tag{B5}$$

$$V(\zeta) = -H(\zeta - \mu) + V_0 \tag{B6}$$

The bending moment is given as

$$M(\zeta) = L \int_0^{\zeta} V(\tau)\, d\tau + M_0 \tag{B7}$$

$$M(\zeta) = L \int_0^{\zeta} -H(\tau - \mu)\, d\tau + M_0 \tag{B8}$$

$$M(\zeta) = L\left[-(\xi - \mu)H(\zeta - \mu) + V_0\xi\right] + M_0 \tag{B9}$$

The angle of deflection can be simplified

$$\theta(\zeta) = L \int_0^{\zeta} \frac{M(\tau)}{EI}\, d\tau + \theta_0 \tag{B10}$$

$$\theta(\xi) = \frac{L^2}{EI} \int_0^{\zeta} \Big[-(\tau-\mu)H(\tau-\mu) + V_o\tau + \frac{1}{L}M_0\zeta \Big]\, d\tau + \theta_0 \tag{B11}$$

$$\theta(\xi) = \frac{L^2}{EI} \int_0^{\zeta} \Big[-\frac{1}{2}(\xi-\mu)^2 H(\xi-\mu) + \frac{1}{2}V_0\xi^2 + \frac{1}{L}M_0\zeta \Big] + \theta_0 \tag{B12}$$

$$\theta(\xi) = \frac{L^2}{2EI} \Big[-(\xi-\mu)^2 H(\xi-\mu) + V_0\xi^2 + \frac{2}{L}M_0\zeta \Big] + \theta_0 \tag{B13}$$

Finally, the deflection is calculated in the form

$$u(\xi) = L\int_0^{\zeta} \theta(\tau)\, d\tau - \frac{1}{GA_S}\int_0^{\zeta} V(\tau)\, d\tau + u_0 \tag{B14}$$

$$\begin{aligned} u(\xi) = &\frac{L^3}{2EI} \int_0^{\zeta} \Big[-(\tau-\mu)^2 H(\tau-\mu) + V_0\tau^2 + \frac{2}{L}M_0\tau + \frac{2EI}{L^2}\theta_0 \Big] d\tau \\ &- \frac{1}{GA_S}\int_0^{\zeta} \big[-H(\zeta-\mu) + V_0 \big] d\tau + u_0 \end{aligned} \tag{B15}$$

$$\begin{aligned} u(\xi) = &\frac{L^3}{2EI} \Big[-\frac{1}{3}(\zeta-\mu)^2 H(\zeta-\mu) + \frac{1}{3}V_0\zeta^2 + \frac{1}{L}M_0\zeta^2 + \frac{2EI}{L^2}\theta_0\zeta \Big] \\ &+ \frac{1}{GA_S}\left[(\zeta-\mu)H(\zeta-\mu) - V_0\zeta \right] + u_0 \end{aligned} \tag{B16}$$

$$u(\xi) = \frac{L^3}{2EI}\left[-(\zeta-\mu)^3 H(\zeta-\mu) + V_0\zeta^2 + \frac{3}{L}M_0\zeta^2\right] + \frac{1}{GA_S}\left[(\zeta-\mu)H(\zeta-\mu) - V_0\zeta\right] + L\theta_0\zeta + u_0 \tag{B17}$$

where G is shear modulus of material property and A_S is cross-section shear area along longitudinal axis. In terms of the deflection expression, Eq. B17, the first part of the equation is the deflection for the Euler-Bernoulli beam. The second part is the shear deformation from Green's function. The schema of installation for DMA experiment is shown in Figure B.2.

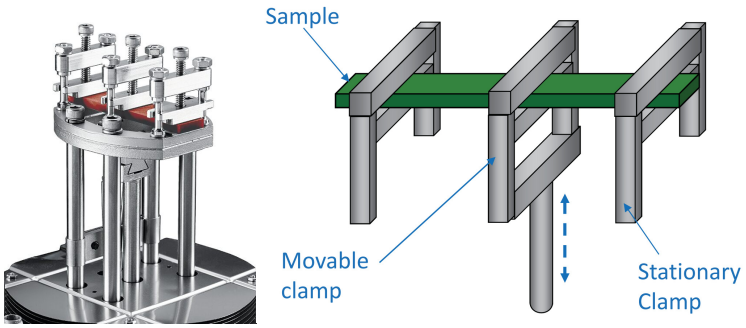

Figure B.2: The bending mechanism in the DMA

B.2 Calculation Theorem and Results

The properties of TPU were determined by DMA (TA Q800). This is a technique in which a beam (sample dimension is 60×10×5 mm, effective length of bending is 35 mm) is placed in dual-cantilever clamps and subjected to a cyclic deformation (Figure B.2). The machine outputs modulus (E' and E''), loss tangent (tan δ), stress, temperature and frequency which are calculated from the amplitude and phase of the force and displacement. Isothermal frequency sweeps were performed at 2 C intervals between -50 C to 80 C , and frequencies 0.5, 2, 5, 10 Hz. The displacement amplitude

was 30 μm. An example of phase retardation between force and deflection in DMA experiment is shown in Figure B.3.

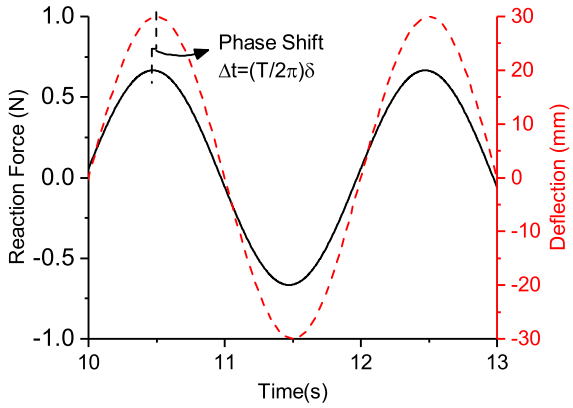

Figure B.3: The DMA experimental phase retardation between force and deflection at 1 Hz frequency

The clamp device in Figure B.3 can be simplified as a beam under centeral loading. Substituting $V_0 = 1/2$, $M_0 = -L/8$, $\theta_0 = 0$, $\mu_0 = 0$ as the boundary conditions; $\zeta = 1/2$, $\mu = 1/2$ as the loading conditions, into Green's functions, the deflection expression is calculated as

$$u\left(\frac{1}{2}\right) = \left[\frac{L^3}{192EI}\right] + \left[\frac{L}{4GA_S}\right]$$

$$\text{where } G = \frac{E}{2(1+\upsilon)}, A_S = \frac{bd}{2} \tag{B18}$$

Substituting the loading into this equation, and further substituting shear modulus G and shear area A_S, giving the full deflection expression

$$u = \left(\frac{L^3}{192EI} + \frac{3L}{2bdE}\right) W \tag{B19}$$

where u is the resultant bending deflection when force W acts on the centre; E, G are Young's modulus and shear modulus respectively; A_S is the cross-section shear area along longitudinal axis, ν is Poisson's ratio, and I is the second moment of area. Shear-bending-curvature of the bending equation, the first term $PL^3/192EI$ is the derivative from Euler–Bernoulli theory, representing force-bending-curvature, while the second term $PL/4GA_S$ relates to the shear effect along the neutral axis in length, representing shear-bending-curvature. Re-writing the equation gives the force response in terms of the deflection and the complex modulus

$$W = \frac{u}{\left(\frac{L^3}{192I} + \frac{3L}{2bd}\right)} E^* \tag{B20}$$

where E^* is the complex modulus value for the viscoelastic material.

For a viscoelastic material undergoing cyclic deformation, the stress is found to lag behind the strain, with a phase shift δ which depends on the complex modulus and frequency of applied loading.

To express the dynamic stress and strain responses, we write the strain and stress as

$$\varepsilon = \varepsilon_0^* e^{i\omega_0 t} \tag{B21}$$

$$\sigma = \sigma_0^* e^{i\omega_0 t} \tag{B22}$$

For a one-term Standard Linear Solid Model, the modulus is given as

$$E^* = \frac{\varepsilon^*}{\sigma^*} = \left[E_0 + E_1 \frac{\tau^2 {\omega_0}^2}{1 + \tau^2 {\omega_0}^2}\right] + i \left[E_1 \frac{\tau \omega_0}{1 + \tau^2 {\omega_0}^2}\right] \tag{B23}$$

So that,

$$E' = \left[E_0 + E_1 \frac{\tau^2 {\omega_0}^2}{1 + \tau^2 {\omega_0}^2} \right] \tag{B24}$$

$$E'' = \left[E_1 \frac{\tau \omega_0}{1 + \tau^2 {\omega_0}^2} \right] \tag{B25}$$

$$\tan \delta = \frac{E'}{E''} \tag{B26}$$

where the E_0 represents the elastic element, while E_1 and τ_1 belong to the Maxwell elements. The equivalent functions of complex modulus for the Generalized Maxwell Model are expressed as

$$E'(\omega) = E_0 + \sum_{i=1}^{m} E_i \frac{{\tau_i}^2 \omega^2}{1 + {\tau_i}^2 \omega^2} \tag{B27}$$

$$E''(\omega) = \sum_{i=1}^{m} E_i \frac{\tau_i \omega}{1 + {\tau_i}^2 \omega^2} \tag{B28}$$

where ω is the frequency of the applied deflection, which is expressed as $\log f$ in the body text. E_0, E_i and τ_i indicate the properties of elements from the Generalized Maxwell Model. We then define the storage and loss moduli as the real and imaginary parts of the complex modulus during the dynamic harmonic cyclic loading. The phase shift factor $\tan \delta = E'/E''$ is the ratio of imaginary modulus to real modulus and represents the lag between strain-stress responses.

The calibrated model for the complex modulus can then be substituted into Eq. B20 to give the relationship between displacement, load and time.

B.3 FE Model Validation

A FE model in compression (Figure B.4) was meshed using C3D8I elements, with 5 elements through the thickness of the specimen. The model has fixed bottom plate (ENCASTRE), while the top plate was driven under velocity control to achieve uniaxial compression at strain rates 0.09, 0.009, 0.0009, 0.08, 0.008 and 0.0008 s^{-1}. The simulation was compared to the results from analytical implementation of the Generalized Maxwell Model using 61 legs of Prony series at reference temperature of 25 C. Figure B.5 exhibits the same strain-stress response in both FE model and analytical Models.

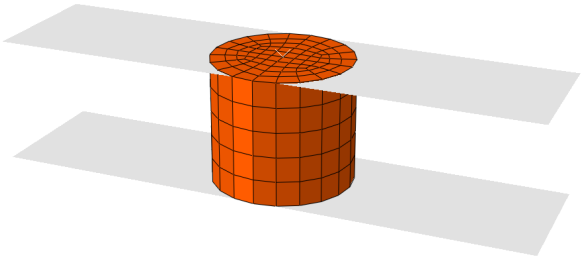

Figure B.4: FE model in compression to validate the implementation of the Generalized Maxwell Model.

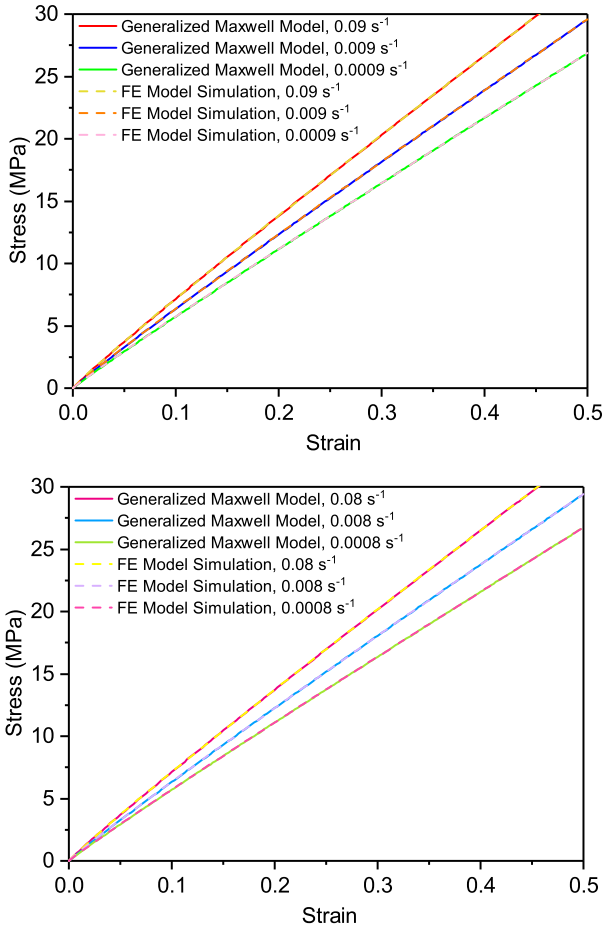

Figure B.5: FE and analytical implementations of the Generalised Maxwell Model at different strain rates.

C Full Set of Experimental Data

C.1 Introduction

TPU is a relatively soft elastomer which has mechanical properties that are easily affected by experimental technique. In addition, certain systematic and experimental errors are inevitable, such as ambient temperature changes, contact problems, as well as the inherent property variations from manufacture. The extensometer accessories (Figure C.1) and digital image correlation (DIC) analysis (Figure C.2) were simultaneously implemented in both compression and tensile tests to validate the experimental data obtained.

In compression experiments, the test sample, a rubber cylinder, has an aspect ratio of 1 to reduce any possible buckling or barrelling during the loading. However, the asymmetrical barrelling shown in Figure C.3 generally happened when true strain was above 0.4.

In quasi-static tests, the imperfection of alignment in load cell and clamps could affect the loading results. Particularly in tensile tests, tearing may occur in the clamp which would seriously affect the strain rate control. To eliminate these errors, an extra extensometer travelling along the compression or tensile axis was implemented into the INSTRON in order to valid the accuracy of strain data obtained from DIC analysis. Figure C.4 indicates the experimental strain rate was only maintained up to 0.35 due to the difficulty in clamping samples at large extensions. This is the main reason that we only took results up to 0.35 strain in cyclic tensile experiments. Experiments were performed 3-5 times for each compression and tensile condition, and the temperature was recorded each time for use in further calculation and analysis.

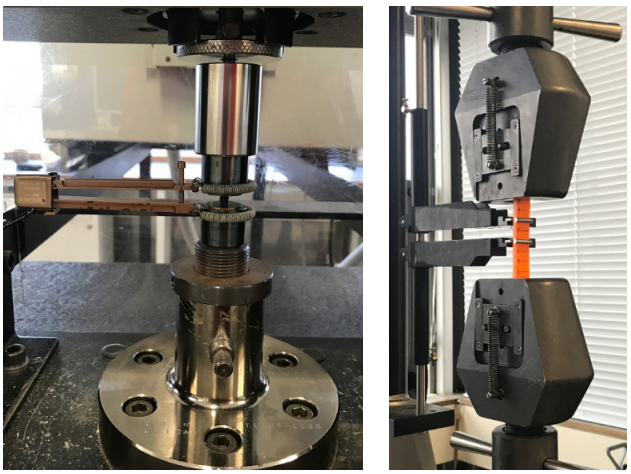

Figure C.1: The extensometer used in quasi-static tests

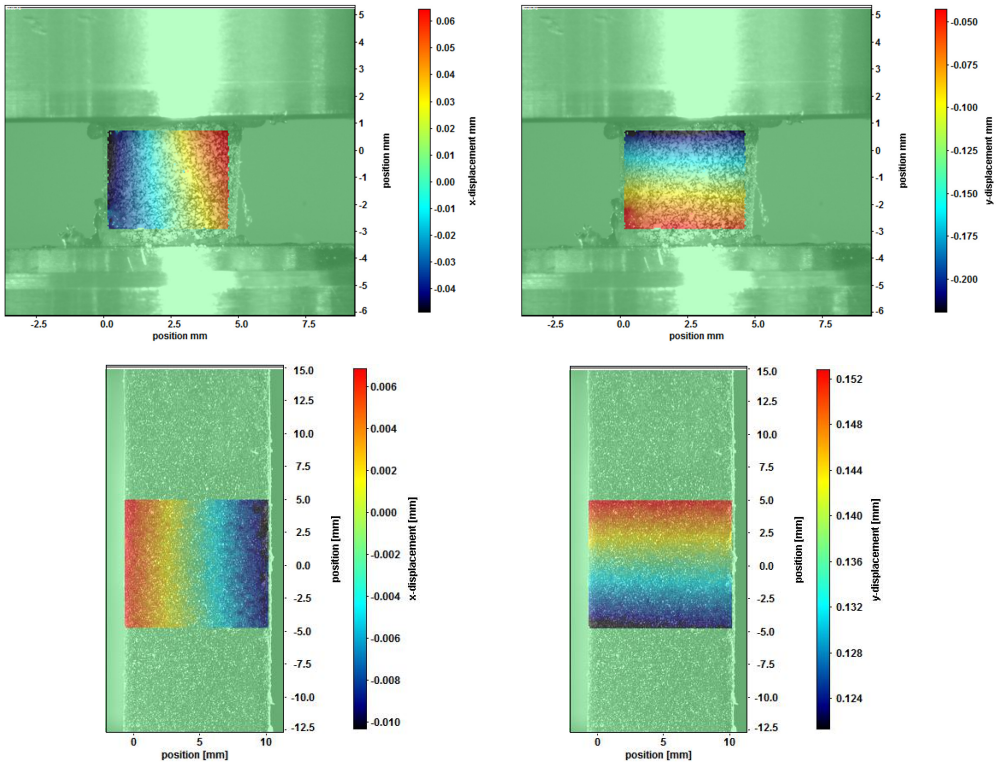

Figure C.2: Use of DIC to confirm strains in quasi-static tests

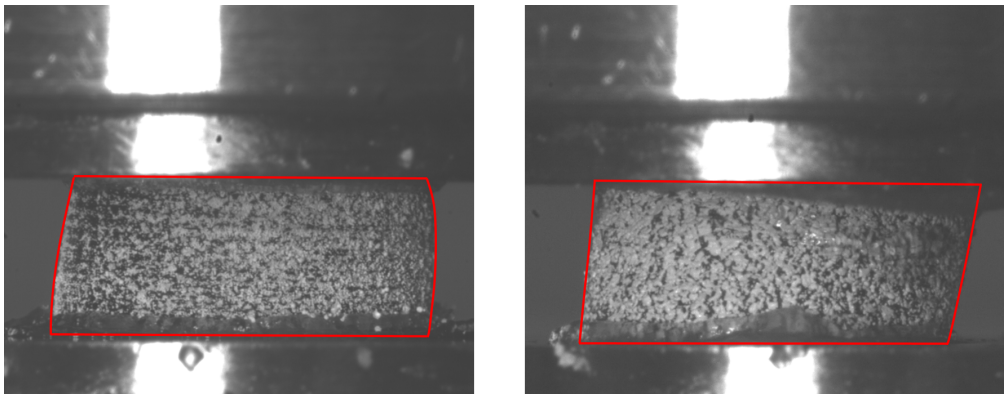

Figure C.3: Asymmetrical barrelling deformation occurred in compression experiments state the strain here

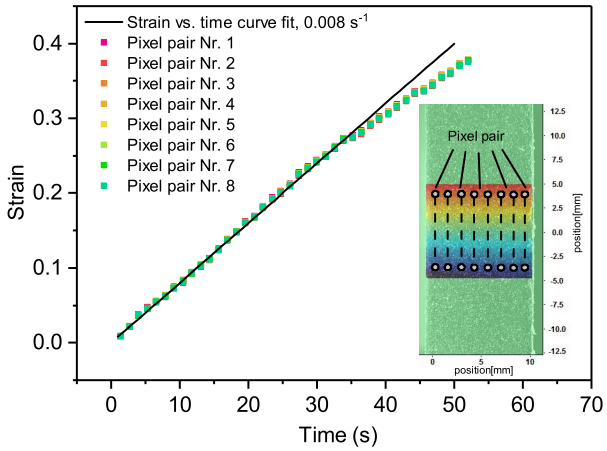

Figure C.4: DIC implementated into strain rate calculationb: the mean of 50 pixel-to-pixel extensions against time indicates that the strain rate can only be maintained up to 0.35 strain in tensile experiments. Here, pixel-to-pixel extensions of 8 pairs of pixels are shown for schema.

C.2 Results

Full sets of data from quasi-static tensile and compression tests are shown in Figure C.5, Figure C.6 and Figure C.7. At least three experiments with virgin sample were performed at each strain rate. The test data closest to the mean value were used in the main text of the paper. The simulation plots based on continuous damage theory were analysed, plotted and compared to other experimental results to examine the validity of the viscoelastic damage model.

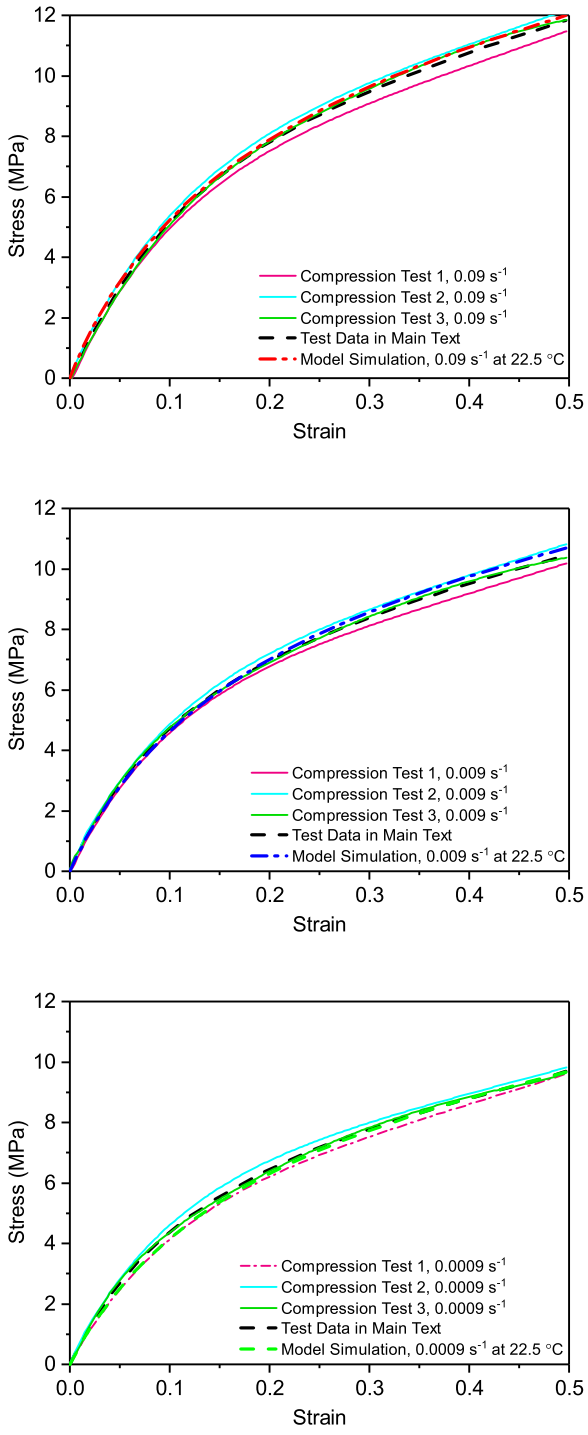

Figure C.5: The quasi-static compression tests data and calibration results for Figure 9 in main text

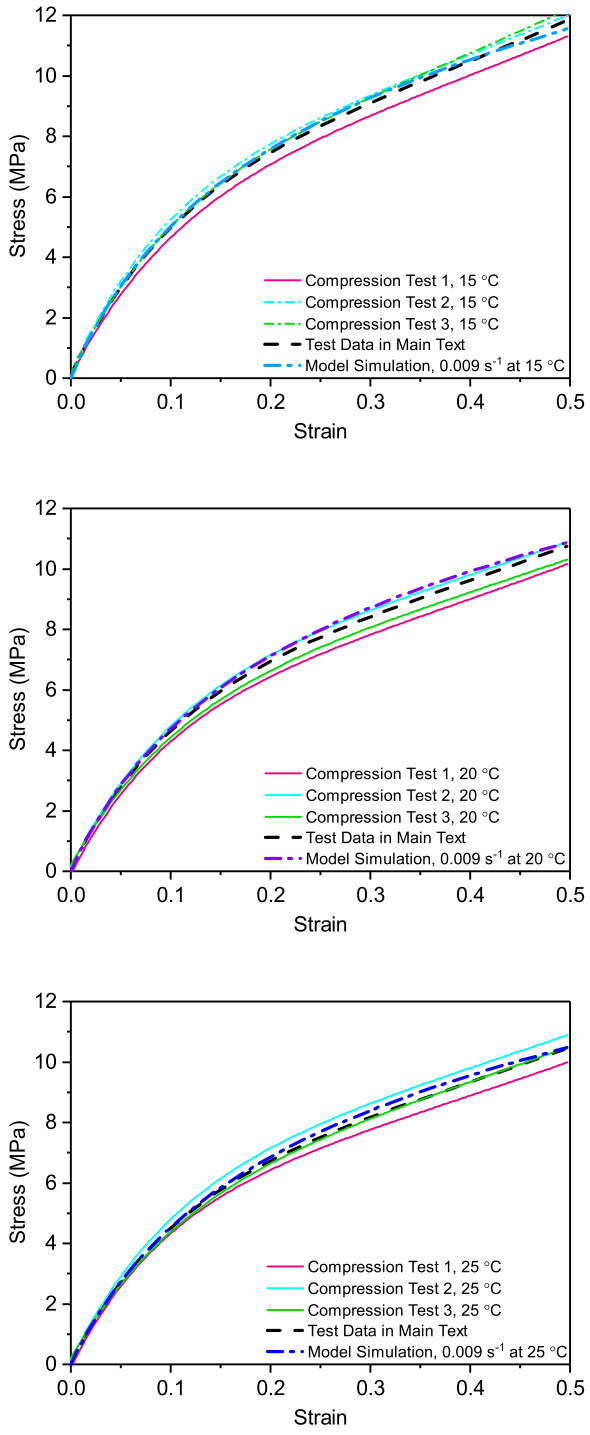

Figure C.6: The quasi-static compression tests data and calibration results for Figure 10 in main text

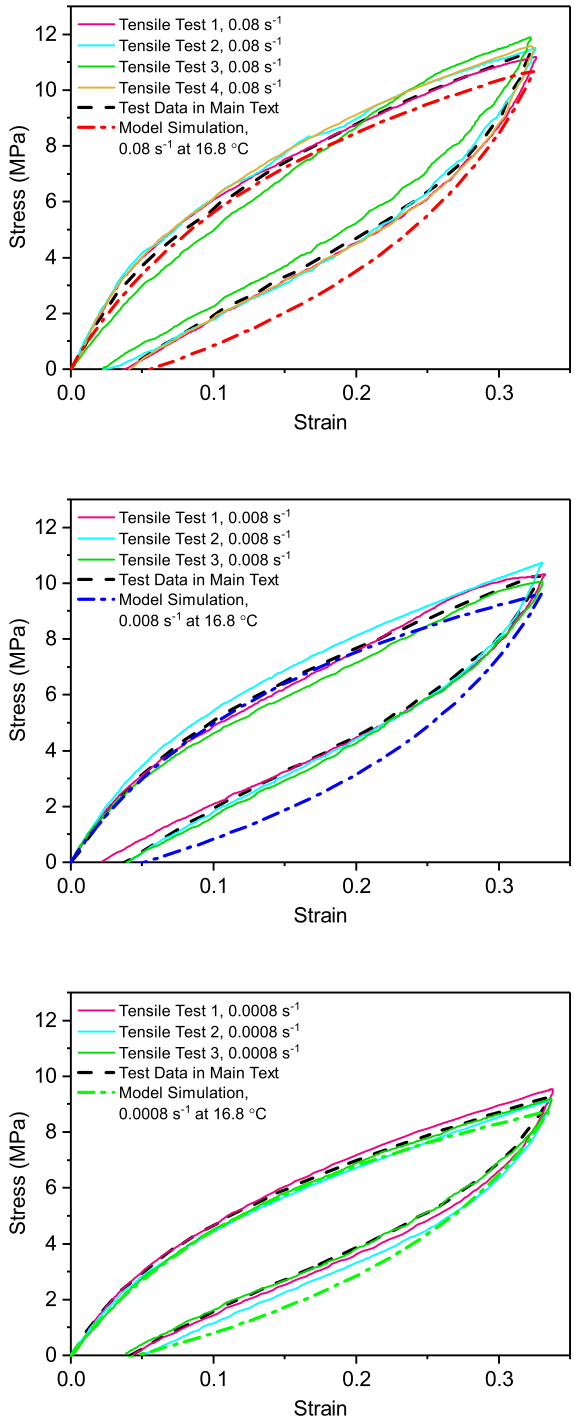

Figure C.7: The quasi-static tensile tests data and calibration results for Figure 11 in main text

References

[1] Ward I.M and Hadley D.W. *An introduction to the mechanical properties of solid polymers*. 1993.

[2] Aamer H. Introduction to Timoshenko Beam Theory. *North South University,* CEED CEE, (211):1–25, 2015.